ROYAL SOCIETY
OF CHEMISTRY

PAPER

Check for updates

Slow-release pesticide microparticles from polylactic acid and emamectin benzoate: preparation and characteristics

Do Van Cong, [ID] *[ab] Nguyen Vu Giang,[ab] Tran Huu Trung,[a] Le Dang Quang,[a] Nguyen Thi Thu Trang,[a] Do Quang Tham,[a] Tran Thi Mai[a] and Nguyen Thi Huong[c]

Emamectin benzoate (EMB) is a potent biological pesticide with broad-spectrum activity against various insects and fungi; however, its practical application is limited due to rapid degradation under UV irradiation, sunlight, and elevated temperatures. In this study, EMB was successfully encapsulated into polylactic acid (PLA) microparticles to enhance its stability, prolong its activity, and improve utilization efficiency. The effects of initial EMB content, PLA solution concentration, and particularly surfactant composition on the microparticle characteristics were systematically investigated. The optimized conditions yielded uniform microparticles with an average diameter of 3.24 μm, a loading content (LC) of 28.74%, and an encapsulation efficiency (EE) of 86.23%. The encapsulation markedly improved both UV and thermal stability of EMB, while *in vitro* release studies demonstrated a significantly sustained and controllable release profile compared with free EMB. These results suggest that PLA-based encapsulation provides an efficient delivery system for EMB, offering potential as a smart pesticide formulation to support sustainable agricultural practices.

1. Introduction

Over the past decades, pesticides have played a crucial role in agricultural production, helping to mitigate pest damage and increase crop productivity and yield. It has been reported that pesticides can prevent production losses in cereals, vegetables, and fruits by up to 32%, 54%, and 78%, respectively.[1] Overall, pesticides are involved in the production of nearly one-third of agricultural products and make a substantial contribution to global food security. However, only a small fraction of applied pesticides, approximately 25%, and in some cases less than 0.1%, actually reaches the target pests and achieves the desired effect.[2,3] This inefficiency arises from factors such as poor water solubility, evaporation, and degradation by heat, sunlight, and UV radiation. As a result, pesticide utilization efficiency remains low, necessitating higher application doses to achieve effective pest control. The excess residues inevitably disperse into the environment, contaminating soil, water, and air, and may even accumulate within plants.

Most pesticides in use today are chemically synthesized (synthetic pesticides) and are relatively persistent under common environmental conditions, making them difficult to

degrade. Consequently, they can exert adverse impacts on ecosystems (soil, water, and air), animals, and plants. To address these drawbacks, biopesticides have increasingly been promoted as sustainable alternatives. They are cost-effective, efficient, and environmentally friendly, leaving minimal harmful residues. Among biopesticides, emamectin benzoate (EMB) has gained wide application because of its broad-spectrum activity and high effectiveness against many insect pests.[4,5] EMB is derived from avermectin B1 through fermentation by the soil microorganism *Streptomyces avermitilis*. It is a macrocyclic lactone, chemically named (4″R)-4″-deoxy-4″-(methylamino)-avermectin B1 benzoate. Compared with avermectin, EMB contains a higher proportion of avermectin B1a, which confers 1–3 orders of magnitude greater and more sustainable insecticidal activity.[6] Despite its relative stability in aqueous solutions at pH 5–8, EMB is highly sensitive to sunlight and UV radiation.[7,8] Prolonged exposure leads to rapid decomposition and loss of biological activity, significantly limiting its practical applications.

Encapsulation of EMB within polymeric carriers has emerged as an effective strategy to overcome these limitations. This approach enables the fabrication of nano- and/or micro-structured formulations with controlled slow-release behavior. Encapsulation not only enhances EMB stability against light-induced degradation, thereby prolonging insecticidal activity, but also improves dispersibility and adhesion to target insects due to reduced particle size and increased surface area.[9–12] Furthermore, controlled release lowers the required pesticide

[a]Institute of Materials Science, Vietnam Academy of Science and Technology, Hanoi, Vietnam. E-mail: dvcong@ism.vast.vn; dovancongktnd@gmail.com

[b]Graduate University of Science and Technology, Vietnam Academy of Science and Technology, Hanoi, Vietnam

[c]Faculty of Chemical Technology, Hanoi University of Industry, Hanoi, Vietnam

dose, reducing mammalian and human toxicity while broadening the application scope of EMB.[7,13–17] Carrier materials may be synthetic polymers such as poly-ε-caprolactone, polyurethane, polyarylsulfone, and methacrylates, or naturally derived biodegradable polymers, including cellulose derivatives,[18–20] polysaccharides (*e.g.*, chitosan, modified starch, carrageenan, alginate, xanthan gum), and proteins (*e.g.*, zein, casein, collagen, gelatin).[21] Natural biodegradable polymers are particularly attractive because they decompose after use, releasing nutrients that act as fertilizers for plants, thereby minimizing environmental impacts and supporting sustainable agriculture.[22–26] Among them, poly(lactic acid) (PLA) is one of the most widely studied biodegradable thermoplastic polyesters, produced from renewable resources.[27] PLA offers numerous advantages, such as high mechanical strength, excellent transparency, strong barrier properties against flavors and aromas, and good resistance to grease and oils. Consequently, PLA-based materials have been extensively applied in food packaging, biomedicine, and agriculture.[27,28]

In agriculture, several pesticides, including chlorpyrifos,[29] buprofezin,[30] propiconazole,[31] beta-cyhalothrin,[32] atrazine,[33] pyrethrin,[34] spinosad,[35] and lemongrass essential oil,[36] have been encapsulated in PLA-based nano- and/or microformulations for controlled release. A variety of fabrication techniques have been reported, including chemical methods (*e.g.*, interfacial polymerization, polycondensation), physicochemical methods (*e.g.*, coacervation, solvent extraction–evaporation, suspension reticulation), and physical methods (*e.g.*, extrusion, fluidized-bed coating, atomization). Among these, solvent extraction–evaporation (also known as emulsification–solvent evaporation) is most widely used due to its simplicity, ease of operation, and the fact that it requires neither high temperatures nor phase-inducing separation agents.[29–37] Surfactants play a crucial role in this method, governing the formation, size, stability, and encapsulation efficiency (EE) of micro- and nanoparticles, especially when combined with ultrasonic or shear-based emulsification.[21,37,38] This method has also been applied to encapsulate EMB into PLA-based systems.

Using a conventional oil-in-water (O/W) emulsion method, Wang *et al.* demonstrated the critical role of surfactants in fabricating EMB slow-release PLA microspheres.[39] Their study showed that combining polyvinyl alcohol (PVA) with other surfactants improved surface activity, enhanced droplet dispersibility, and reduced particle size. Among ten co-surfactants tested, EL-40, span 60, tween 80, span 80, tween 60, emulsifier 500, emulsifier 600, emulsifier 700, emulsifier 1601, and AEO-9, EL-40 (polyoxymethylene castor oil), a nonionic surfactant, was identified as the most suitable when paired with PVA. This combination produced uniform nanospheres with an average diameter of ∼320.5 nm, an EMB loading content (LC) of ∼40.8%, and an EE of ∼83.2%. However, fabrication conditions such as PLA solution concentration, EMB/PLA feed ratio, and homogenization speed were not reported. Yin *et al.* fabricated EMB-loaded PLA microspheres using a mixture of sodium dodecyl benzene sulfonate (SDBS, 2% w v^{-1}) and gelatin (0.5% w v^{-1}) as surfactants.[8] The resulting microspheres had diameters ranging from 9 to 42 μm, depending on PLA solution

concentration (6 and 9 wt%), emulsifier concentration (0.5–2%), and emulsification time (1–2 h). Although EE was relatively high (88.30–94.42%), LC remained low (13–14%) due to the low EMB/PLA feed ratio (25/100 w/w). Such low LC may reduce insecticidal efficiency and limit practical application. Zhang *et al.* improved the traditional emulsion–solvent evaporation method by introducing water-miscible organic solvents (*n*-butanol, diethyl ether, ethyl acetate, or acetone) into the oil phase and ethanol into the aqueous gelatin phase.[40] This modification accelerated microsphere formation, reduced particle size, minimized EMB loss into the aqueous phase, and improved LC. Particle diameter decreased in the order diethyl ether > acetone > ethyl acetate > *n*-butanol. LC and EE reached maximum values of 31.8% and 92.7%, respectively, when acetone was added. Interestingly, ethanol addition decreased both LC and EE despite reducing particle size from 14.4 to 6.82 μm. Emulsification speed also had a strong effect: increasing the speed from 6000 to 9000 rpm reduced mean particle size from 14.4 to 6.02 μm but lowered EE from 79.2% to 60.1%. Recently, Xu *et al.* further optimized this modified method by adjusting PLA concentration, homogenization rate, oil/water ratio, and core/shell ratio.[9] Using a mixed organic solvent (methylene chloride and acetone) for the oil phase, gelatin as the internal aqueous phase, and distilled water as the external aqueous phase, they achieved EMB microspheres with an EE exceeding 90%. Compared with conventional solvent evaporation, this method improved EE by more than 30%, reaching a maximum of 90.63%. Collectively, these studies show that encapsulating EMB in PLA-based nano- and microspheres involves more than technical optimization; it requires balancing polymer–surfactant interactions, solvent dynamics, emulsification kinetics, and drug-matrix affinity. Several theoretical insights can be drawn: (i) synergistic use of dual surfactants (*e.g.*, PVA with EL-40 or gelatin with SDBS) enhances emulsion stability and allows better control over particle size and EE; (ii) solvent polarity and miscibility strongly influence mass transfer during solvent evaporation, affecting both LC and EE; and (iii) homogenization speed critically determines droplet breakup, particle nucleation, and polymer solidification. These findings highlight that both thermodynamic factors (phase miscibility, polymer–drug compatibility) and kinetic parameters (shear rate, solvent diffusion rate) govern the structure–property relationships of EMB–PLA microspheres.

Building on this background, the present work investigates the effects of gelatin, PVA, sodium dodecyl sulfate (SDS), and particularly their binary mixtures on EMB encapsulation in PLA microspheres. These combinations, not previously reported, are expected to provide novel and effective surfactant systems. Additionally, the effects of PLA solution concentration and EMB feed ratio were examined to improve LC and EE while reducing particle size. Thermal analysis (TGA and DSC), UV stability, and release studies were also conducted to assess PLA–EMB interactions and to gain further insight into encapsulation performance.

2. Methods and characterization

2.1. Preparation of microparticles. Previous studies have demonstrated that PVA and gelatin are two effective surfactants for producing EMB-loaded PLA nano- and/or microspheres.[9,40] In addition, a combination of gelatin and sodium dodecyl benzene sulfonate (SDBS) has also been employed as an emulsifier and stabilizer for such microspheres.[8] In this work, individual surfactants (SDS, PVA, gelatin) as well as binary mixtures (gelatin/PVA, SDS/PVA, SDS/gelatin) were employed as emulsifiers and stabilizers for microparticle formation. Briefly, EMB and PLA were dissolved in 25 mL of dichloromethane (DCM) to obtain the oil phase (O). The aqueous phase (W) was prepared by dissolving the designated surfactant(s) in 150 mL of deionized water.[41] The O phase was then slowly added dropwise into the W phase under vigorous magnetic stirring (500 rpm), forming an oil-in-water (O/W) emulsion. Subsequently, the emulsion was homogenized using a SHG-15A Sci Lab homogenizer at 8000 rpm for 6 min, and then maintained under continuous magnetic stirring for 4 h to ensure homogenization and solvent evaporation. During this process, PLA microparticles were gradually formed.

To prevent EMB degradation by light and heat, the reaction vessel was covered with black nylon and kept in an ice-water bath throughout the procedure. The resulting suspension was centrifuged at 5800 rpm for 6 min to collect solid microparticles, which were then washed with deionized water and centrifuged three times to remove residual DCM. Finally, the purified microparticles were lyophilized using an Epsilon 1-4LSC freeze-dryer (Germany) for 24 h to obtain dry solids. The components used in the fabrication and their roles are summarized in Table 1.

2.2. Characterization

Digital microscope images: a digital microscope was used to observe the shape and size of the particle and was performed on a VHX-970F device (Keyence, Japan).

Scanning Electron Microscope (SEM): SEM images were captured by using JEOL JSM-6510LV instrument (Japan), samples were covered silver before capture.

Dynamic light scattering measurement (DLS): Dynamic light scattering (DLS) was performed on a DLS SZ-100Z2 device (Horiba, Japan). About 0.10 g of microspheres were put into the glass beaker filled with 20 mL of distilled water under ultrasonic condition by and the mixture was sonicated at 750 W for 2 minutes using a VCX750 machine (Sonics, USA) and statically kept for 2 minutes before conducting DLS measurements. The mean diameter of microspheres was the diameter of 50% of the microspheres, while the span was calculated by following equation:[7]

$$\text{Span} = \frac{\text{D90} - \text{D10}}{\text{D50}} \tag{1}$$

Where, D90 and D10 represents the diameter of 90% and 10% the microspheres.

Fourier transform infrared spectroscopy (FTIR): FTIR spectra of samples were measured on a Nicolet iS10 infrared spectrometer (UK) according to the reflectometry method and was performed at room temperature in the range of 400–4000 cm^{-1} with a scanning number of 16 times, a resolution of 8 cm^{-1}.

Table 1 Ingredients and roles in the fabrication of PLA microspheres loaded with EMB

Ingredients	Role	Sample symbols
EMB	Active ingredient – pesticide	
PLA	Carrier (biodegradable biopolymer), forming a micro spherical shell around EMB.	
Dichloromethane (DCM)	Organic solvent to dissolve PLA and EMB, creating an organic phase in the emulsion. The PLA solution concentration was varied from 10% to 2%, while the feeding EMB/PLA weight ratio was adjusted to 30/100, 50/100, 70/100, and 90/100	
Stirrer (high speed) and homogenizer	Creates shear force to disperse the organic phase into small droplets in water, forming the desired size of microspheres. The stirrer speed was fixed at 500 rpm and the homogenizing rate was kept at 8000 rpm in 6 minutes. Emulsification time lasted about 4 hours	
PVA	Emulsifier (surfactants and co-surfactants),	P
Gelatin	stabilizing the emulsion system (aqueous	G
SDS	phase), preventing agglomeration during the	S
Gelatin/PVA mixtures	microspheres formation process. The weight	M1
SDS/PVA mixtures	ratio of gelatin/PVA, SDS/PVA and SDS/gelatin	M2
SDS/Gelatin mixtures	was kept at 20/80 w/w	M3
Distilled water (diluted water)	Continuously mixed in the W/O emulsion system, helping to form microspheres. The volume ratio of oil phase/water phase is fixed constant at 1/6	

UV-Vis spectroscopy: UV-Vis spectroscopy measurements was performed on a Biochrom S80 machine (Biochrom – United Kingdom) at the wavelength range of 200–800 nm.

Thermogravimetric analysis (TGA): TGA measurements was conducted on TGA 209F instrument (Netsch, Germany) with heating rate 10 °C minute⁻¹, from room temperature to 700 °C under nitrogen atmosphere.

Differential scanning calorimetry (DSC): DSC measurements was carried out by using DSC 204F1 instrument (Netsch – Germany), heating rate and cooling rate 10 °C minute, from room temperature to 300 °C under nitrogen atmosphere.

Determination of EMB loading content (LC) and encapsulation efficiency (EE): UV-Vis measurement was used to determine LC and EE with absolute ethanol as a solvent. Quantification was performed by establishing a calibration curve of the relationship between the adsorption and concentration of EMB in absolute ethanol in the concentration range of 10–90 mg L⁻¹ with the determination assay described in the SI File.

In vitro release testing: the *in vitro* release test was performed in the two environments including in absolute ethanol and the alcohol solution 50° as described in the SI File and Wang *et al.* reported.[42]

UV and thermal stabilities: the EMB loaded PLA microspheres were put into the glass tubes and UV tested under a fluorescent lamp UVA-340 with average wavelength 340 nm at 25 °C for 7 days. This test was conducted following GB/T 19136–2003 as reported by Yin and Wang *et al.*[8,39] The other glass tubes contained the pesticide loaded microspheres was stored at 54 °C in the chamber for 14 days according to Accelerated Storage Test CIPAC MT 46.4 (CIPAC 5217/R).[8,39] The content changes of EMB in the microspheres *versus* time intervals were determined indirectly by UV-Vis measurement.

3. Results and discussion

3.1. Optimization of some factors affecting the fabrication process of EMB-loading PLA microparticles

3.1.1. Effects of surfactant concentrations. In the oil-in-water (O/W) emulsion–solvent evaporation method, surfactants are essential for reducing surface tension, stabilizing droplets, and preventing coalescence, thereby enabling microparticle formation.[43] Once droplets are generated, surfactant molecules adsorb at their interface to form a protective layer that hinders aggregation (Fig. S1). This stabilization results in smaller droplets and, consequently, smaller microparticles. Thus, surfactants exert a decisive influence on the formation, particle size, and dispersion of PLA microparticles.[21,37,38,43,44] Without surfactant, no particles were obtained, confirming their necessity (Fig. S2a).

For PVA, although higher PVA levels lower surface tension, however, the simultaneous increase in solution viscosity hinders efficient dispersion of oil droplets in the aqueous phase and slows microparticle formation.[45] Thus, larger microparticles formed at higher PVA concentrations, while the smallest particles were obtained at 1% PVA (Fig. S2b–d). In contrast, gelatin concentration had little effect on particle size, as digital microscopy showed (Fig. S3). This is likely because gelatin

causes only minor changes in surface tension with concentration, resulting in negligible influence on droplet breakup and particle formation.[46] Overall, 1% surfactant concentration was found to be optimal for microparticle preparation and was therefore applied to other surfactants in subsequent studies.

3.1.2. Effect of different types of surfactants. Fig. 1 presents SEM images of EMB-loaded PLA microparticles prepared with different surfactants, showing clear morphology differences. With SDS (sample S), irregular rod- and strip-like fragments dominated, along with large microspheres (∼60–80 μm, Fig. 1a and b).

In contrast, both gelatin (sample G) and PVA (sample P) promoted the formation of predominantly spherical microparticles. Gelatin-derived microparticles displayed diameters ranging from 10 to 50 μm with rough and porous surfaces (Fig. 1c and d), whereas PVA-derived microparticles exhibited smaller diameters of 10–40 μm and relatively smooth surfaces (Fig. 1e and f). The observed differences can be attributed to the nature of the surfactants: SDS, a strong ionic surfactant, drastically reduced surface tension and accelerated DCM evaporation, leading to rapid polymer precipitation, poor droplet dispersion, and the formation of larger, irregular structures. Meanwhile, the milder, the nonionic surfactants (gelatin, PVA) reduced surface tension more moderately, allowing slower granulation and finer dispersion, ultimately yielding smaller and more uniform microspheres. These results highlight
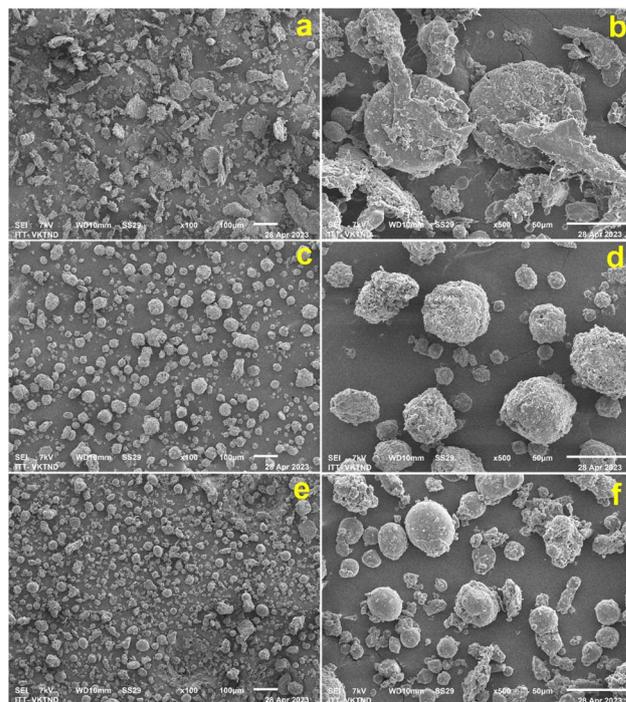
Fig. 1 SEM images of EMB–loaded PLA microparticles prepared with different surfactants: (a and b) SDS (sample S), (c and d) gelatin (sample G), and (e and f) PVA (sample P). Images were taken at ×100 (left) and ×500 (right) magnification respective scale bars 100 μm and 50 μm. The PLA solution concentration was 10% and the EMB/PLA feed ratio was 50/100 (w/w). SEM conditions: 7 kV accelerating voltage.

gelatin and PVA as more suitable surfactants than SDS for fabricating EMB-loaded PLA microparticles.

Previous studies (Morsy *et al.*) have indicated that the addition of multiple surfactants can reduce recoalescence and, in some cases, lower surface tension more effectively than the individual surfactants alone. Moreover, surfactants dissolved in the dispersed phase rather than the continuous phase can facilitate the formation of smaller microparticles.[43,44] Guided by these findings, dual mixtures of gelatin, PVA, and SDS were investigated. At a 20/80 weight ratio, gelatin/PVA (sample M1) produced microparticles of 15–25 μm, significantly smaller than those from individual surfactants. Their surface resembled gelatin-derived microparticles (sample G), being rough and porous (Fig. 2a and b), unlike earlier reports where gelatin, PVA, and even SDBS/gelatin mixture yielded smooth microspheres.[8,39,40] This difference likely arose from air bubbles introduced by gelatin during emulsification, producing porous structures that may enhance drug loading but accelerate diffusion-controlled release.

In contrast, mixtures containing SDS (M2: SDS/PVA and M3: SDS/gelatin, both 20/80) yielded distorted, irregular particles >50 μm (Fig. 2c–f). The strong ionic behavior of SDS caused drastic surface tension reduction and rapid solvent removal, leading to uncontrolled growth, aggregation, and poor morphology. Taken together, nonionic surfactants (PVA,

gelatin) individually produced uniform microparticles and, in combination, further reduced microparticle size while controlling surface porosity. However, when SDS was included, its strong ionic behavior dominated, resulting in poorer morphology and larger particle sizes. Therefore, binary mixtures of nonionic surfactants, particularly gelatin/PVA, appear to be the most promising approach for fabricating EMB-loaded PLA microparticles with both small size and tunable surface porosity.

For nano- and micro-particle delivery systems, two critical parameters, pesticide loading content (LC) and encapsulation efficiency (EE), are considered alongside microparticle size and morphology. These parameters determine the actual amount of active ingredient incorporated and the effectiveness of its entrapment. In this study, LC and EE were evaluated using UV-Vis spectrophotometry. The obtained results clearly indicate that the choice of surfactant type strongly affects pesticide entrapment. At equal solution concentrations, PVA (P) and gelatin/PVA (M1) microparticles displayed stronger UV-Vis absorption of EMB than gelatin (G) and SDS (S) samples (Fig. S4), consistent with the quantitative data in Table 2. Among the investigated samples, S microparticles exhibited the lowest LC (19.04%) and EE (57.12%) due to the high polarity and poor compatibility of SDS with EMB, which promote diffusion out of the polymer matrix during solidification. Similar reductions were observed in SDS-containing mixtures (M2 and M3), which exhibited clearly reduced LC and EE compared with non-ionic surfactant systems. In contrast, G microparticles reached 23.84% LC and 71.53% EE, while the highest values (∼27% and 81%) were achieved with P and M1. Notably, M1 exhibited slightly higher values than P, confirming the synergistic effect of gelatin addition. As reported by Chi *et al.*, the incorporation of gelatin decreases the viscosity of PVA aqueous solution, thereby facilitating dispersion of the oil phase, reducing microparticle size, and enhancing encapsulation performance.[47] In addition, the structural similarity of gelatin to EMB likely contributes to stronger retention of EMB molecules within the matrix.[9,48] These findings demonstrate that the gelatin/PVA mixture was identified as the most effective surfactant system for enhancing pesticide encapsulation and thus was selected for subsequent experiments.

3.1.3. Effects of feeding EMB/PLA weight ratios. The morphology of the microparticles was strongly influenced by the feeding EMB content. As shown in Fig. 3, neat PLA microparticles exhibited a uniform spherical shape with a smooth
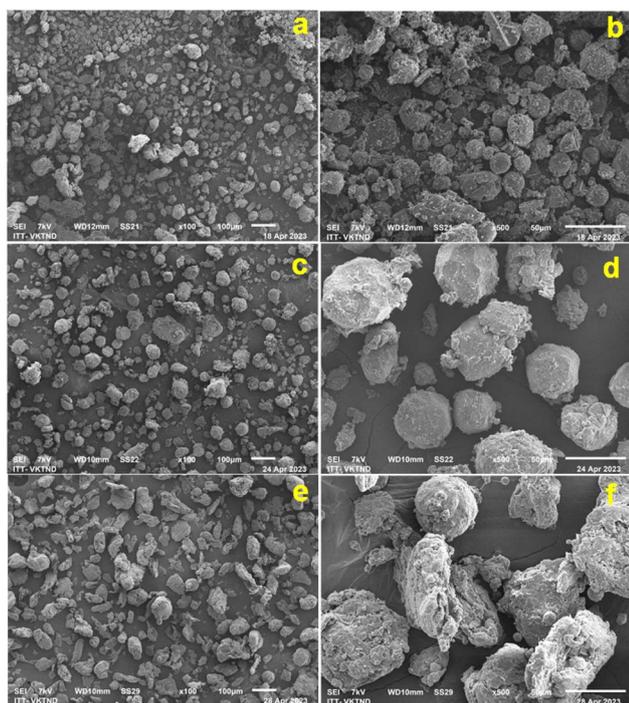

Fig. 2 SEM images of PLA microspheres prepared with dual-surfactant systems: gelatin/PVA (M1, a and b), SDS/PVA (M2, c and d), and SDS/gelatin (M3, e and f). PLA solution concentration was fixed at 10%, and the feeding EMB/PLA weight ratio was maintained at 50/100 wt./wt. Images were taken at ×100 (left) and ×500 (right) magnification respective scale bars 100 μm and 50 μm. The PLA solution concentration was 10% and the EMB/PLA feed ratio was 50/100 (w/w). Scale bar: 50 μm. SEM conditions: 7 kV accelerating voltage.

Table 2 Loading content (LC) and encapsulation efficiency (EE) of EMB-loaded PLA microparticles prepared with different surfactants

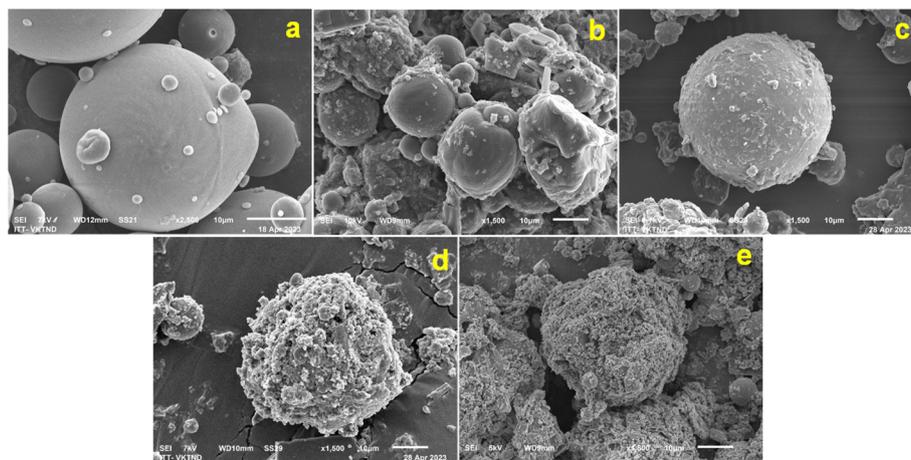| Coded sample	Surfactant	LC, %	EE, %
S	SDS	19.04	57.12
G	Gelatin	23.84	71.53
P	PVA	26.73	80.20
M1	Mixed gelatin and PVA	26.95	80.86
M2	Mixed SDS and PVA	24.38	73.14
M3	Mixed SDS and gelatin	23.92	71.77

Fig. 3 SEM images of PLA microparticles fabricated at different feeding EMB/PLA weight ratios (w/w): (a) 0/100, (b) 30/100, (c) 50/100, (d) 70/100, and (e) 90/100. The PLA solution concentration was fixed at 10%.

surface (Fig. 3a). Upon the addition of EMB, the overall particle size remained almost unchanged; however, numerous tiny particles appeared on the surface, leading to a rougher and more porous morphology. These particles can be attributed to EMB nanoparticles, which were not only encapsulated within the PLA matrix but also deposited on the outer surface of the microparticles. With increasing EMB/PLA weight ratios, the surface roughness of the microparticles became more pronounced due to the greater number of adhered EMB nanoparticles (Fig. 3b–e).

Table 3 summarizes the LC and EE values of PLA microparticles prepared with various EMB/PLA feeding ratios. When the feeding ratio increased from 30/100 (w/w) to 50/100 (w/w), both LC and EE increased markedly. However, further raising the EMB/PLA ratio to 70/100 (w/w) and 90/100 (w/w) resulted in only a slight increase in LC but a sharp decline in EE. This indicates that excessive EMB could not be fully encapsulated due to the limited amount of PLA matrix, leading to the loss of surplus EMB and thus a reduced EE. On the molecular level, the encapsulation of EMB in PLA relies on both physical entrapment during solidification and intermolecular interactions such as van der Waals forces and hydrogen bonding between EMB and the PLA chains. At moderate EMB content ($\leq$50/100 w/w)), EMB molecules can be effectively dispersed within the PLA matrix, stabilized by these interactions. However, when the EMB concentration exceeds the solubility or compatibility limit of PLA, the matrix becomes saturated, resulting in phase separation. The unbound EMB molecules tend to migrate and crystallize on the microparticle surface during solvent evaporation, forming loosely attached nanoparticles. Consequently, the proportion of EMB retained inside the microparticles decreases significantly, leading to lower EE despite a marginal increase in LC.

This observation is consistent with the SEM images, where large amounts of EMB nanoparticles were found adhered to and coated on the microparticle surfaces rather than being encapsulated inside (Fig. 3d and e). Among the tested formulations, the EMB/PLA ratio of 50/100 (w/w) yielded the optimal balance, with relatively high LC (26.95%) and EE (80.86%), and was therefore identified as the most suitable condition for fabricating EMB-loaded PLA microparticles.

3.1.4. Effects of PLA solution concentration. Another critical factor in microparticle fabrication is the PLA concentration

Table 3 Loading content (LC) and encapsulation efficiency (EE) of EMB-loaded PLA microparticles fabricated at different feeding EMB/PLA weight ratios (wt./wt.)

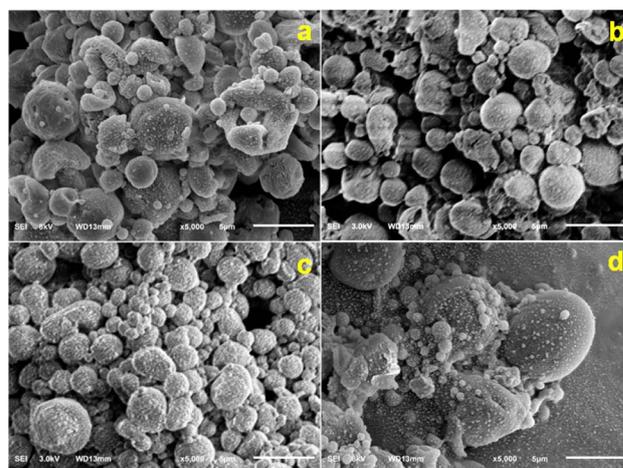| Feeding weight ratio of EMB/PLA (wt./wt.)	LC, %	EE, %
10/100 (9.09%)	7.98	87.79
30/100 (23.08%)	19.36	83.88
50/100 (33.33%)	26.95	80.86
70/100 (41.18%)	27.11	65.83
90/100 (47.37%)	27.48	58.01

Fig. 4 SEM images of EMB-loaded microparticles obtained from PLA solution concentrations of (a) 8%, (b) 6%, (c) 4%, and (d) 2%.

in the oil phase. As shown in Fig. 4, well-defined microspheres were obtained at 4–8% PLA, whereas at 2% the microparticles were incompletely formed and irregular. Increasing PLA concentration strongly affected particle size: at 10% concentration, the mean diameter was ∼25 μm, while decreasing to 8% reduced the size to ∼5 μm, with only slight further decreases at 6% and 4%. DLS results confirmed this trend, giving average diameters of 4.09 μm, 2.84 μm, and 2.22 μm for C8, C6, and C4 samples, respectively (Table 4). Under the same PLA concentration (6%), these sizes are notably smaller than those reported by Yin et al.[8] and Zhang et al.,[40] indicating more efficient size control in our system.

From a molecular perspective, the effect of PLA concentration is closely related to solution viscosity and chain entanglement. At high concentrations (≥10%), extensive chain entanglement markedly increases viscosity, which not only hinders droplet breakup during emulsification but also promotes microparticle aggregation, as reported by Ibadat et al.[49]

This explains why the 10% PLA solution produced excessively large particles, beyond the measurable range of DLS in this study. At 8% PLA, the microparticle size decreased sharply to 4.09 μm but displayed a broad size distribution, with a high polydispersity index (PI > 0.7) and a wide DLS peak (Fig. S5), indicating non-uniformity. This was consistent with the SEM image (Fig. 4a). At very low concentrations (2%), the polymer chain density was insufficient to stabilize droplets, leading to collapsed morphologies. In contrast, intermediate concentrations (4–6%) provided the best balance: reduced viscosity facilitated droplet dispersion, while adequate chain density ensured structural stability. Consequently, the resulting microparticles exhibited the smallest size and highest uniformity, as evidenced by a moderate PI (0.08 < PI ≤ 0.7) and sharp DLS peaks (Fig. S5).

PLA concentration also influenced EMB encapsulation. Reducing the polymer concentration in the oil phase, from 10% to 6%, not only decreased microparticles size but enhanced both LC and EE, owing to smaller droplets with higher surface-to-volume ratios, which promoted more efficient encapsulation of EMB molecules (Table 5). At higher concentrations (≥8%), the increased viscosity of the oil phase hindered the efficient dispersion of droplets in the aqueous phase, resulting in larger and less uniform microparticles with reduced encapsulation efficiency. At concentration of 4% PLA, however, LC and EE began to decline, and at 2% they dropped sharply due to incomplete shell formation and EMB leakage, as also seen in SEM (Fig. 4d). At PLA solution concentration of 6%, the viscosity was moderate enough to allow fine emulsion droplet formation,

while still providing sufficient PLA chains to encapsulate EMB tightly through hydrophobic interactions and physical entanglement. At this concentration, uniform spherical microparticles were produced with the highest LC and EE values, 28.74% and 86.23%, respectively. These results are comparable to those of Zhang et al.[40] but showed over twice the LC reported by Yin et al.,[8] highlighting the superior loading performance of the present system.

Overall, an intermediate concentration (6–8%) provided the best balance between viscosity and chain availability. In particular, 6% PLA produced uniform spherical microparticles with the highest LC (28.74%) and EE (86.23%), outperforming several reported systems. The superior performance at this concentration can be attributed to efficient droplet dispersion, adequate chain coverage, and strong hydrophobic interactions between PLA and EMB.

3.2. Characteristics of the microparticles

3.2.1. FTIR analysis. FTIR analysis (Fig. S6) confirmed the successful encapsulation of EMB within PLA microparticles. Neat PLA exhibited characteristic absorption bands, including the ester C=O stretching at ∼1749 cm^{-1} and the C–O–C stretching at ∼1183 and 1083 cm^{-1}, which are typical for aliphatic polyesters. Pure EMB, by contrast, showed a broad –OH stretching band (∼3154 cm^{-1}), a carbonyl peak at ∼1729 cm^{-1}, and aromatic C=C/C–H vibrations at ∼1596 and 1538 cm^{-1}. In the EMB-loaded PLA microparticles, the spectra contained both sets of characteristic bands, together with additional peaks at ∼1634–1560 cm^{-1} attributed to the aromatic benzoate ring of EMB.[39,50] Furthermore, slight shifts in the –OH, C=O, and C–O–C vibrations compared with the neat components indicate molecular-level interactions, such as hydrogen bonding between the hydroxyl groups of EMB and the carbonyl groups of PLA, as well as dipole–dipole interactions involving C=O and C–O–C groups. These interactions likely contribute to the stabilization of the drug–polymer system and are consistent with the high encapsulation efficiency achieved in the optimized formulation.

3.2.2. Thermal properties. As reported by Panyam et al.,[51] differential scanning calorimetry (DSC) is a powerful tool to investigate the physical state of an encapsulated drug within micro- and nanoparticles. Fig. 5 shows the DSC thermograms of neat EMB, blank PLA microparticles, and EMB-loaded PLA microparticles. Pure EMB exhibited two main endothermic peaks at 150.3 °C and 199.0 °C, corresponding to its melting temperature (T_m) and thermal decomposition temperature (T_d), respectively.[40,52] When EMB was encapsulated into PLA

Table 4 The changes of microsphere sizes *versus* PLA solution concentrations

Concentrations of PLA solution, %	D10 (nm)	D50 (nm)	D90 (nm)	D97 (nm)	Span	Polydispersity index (PI)
8	2837	4092	5223	5901	0.583	0.921
6	1967	2837	3621	4623	0.936	0.659
4	1741	2223	2837	3205	0.659	0.406

Table 5 The LC and EE values of EMB loaded PLA microparticles fabricated from different PLA solution concentrations

Concentrations of PLA solution, g/100 mL	Average diameter, μm	LC, %	EE, %
10	25.30[a]	26.95	80.86
8	4.27[b]	28.15	84.46
6	3.24[b]	28.74	86.23
4	2.10[b]	27.52	82.57
2	Indefinite	20.26	60.79

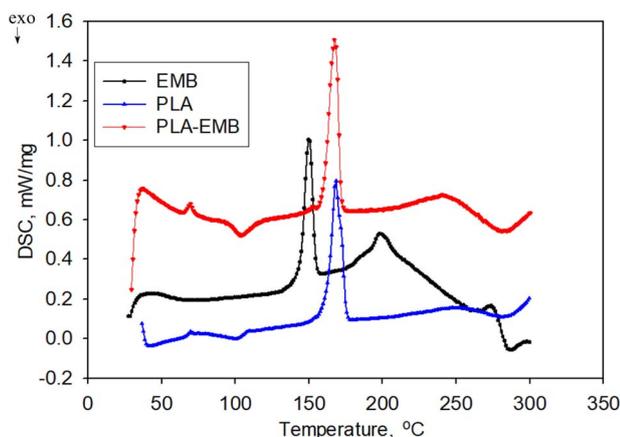[a] Estimated results by SEM observation. [b] Results determined by DLS.

Fig. 5 DSC thermograms of neat EMB, blank PLA microparticles (PLA), and EMB-loaded PLA microparticles (PLA–EMB).

microparticles, the characteristic melting peak of EMB either disappeared or became significantly broadened and reduced in intensity. This phenomenon indicates that EMB was not present as crystalline domains but rather dispersed in an amorphous state within the polymeric matrix. Such a molecularly dispersed distribution can enhance drug–polymer interactions (e.g., hydrogen bonding between EMB hydroxyl groups and PLA carbonyl groups), improve stability, and prevent premature recrystallization. Meanwhile, the thermal profile of the blank PLA microparticles remained unchanged, further confirming that the modification observed in EMB-loaded microparticles originated from the drug encapsulation.

The DSC thermograms of PLA microparticles with and without EMB displayed three thermal transitions at approximately 69 °C, 103 °C, and 167 °C, which correspond to the glass transition temperature (T_g), crystallization temperature (T_c), and melting temperature (T_m) of PLA, respectively. Interestingly, compared with neat PLA microparticles, the T_g and T_c of EMB-loaded PLA microparticles were almost unchanged; however, both the heat capacity (C_p) and the enthalpy change (ΔH) associated with the glass transition and crystallization increased in the presence of EMB (Table 6). According to Zhang et al., such behavior can be attributed to the combination of PLA and active compounds (e.g., EMB) at the amorphous or molecular level, where amorphous PLA provides favorable interactions with EMB, thereby facilitating the encapsulation process

and enhancing the EE.[9,40] where, $\chi_C = \dfrac{\Delta H_m + \Delta H_c}{\Delta H_m^o} \times 100$; ΔH_m^o is the melting enthalpy of a 100% crystalline PLA 93.1 J g^{-1} as reported by Beltrán et al.[53]

A similar trend was observed for the C_p and ΔH of the melting transition. Notably, the characteristic T_m peak of pure EMB did not appear in the DSC thermogram of EMB-loaded PLA microparticles, while the T_m of PLA slightly shifted from 168.4 °C to 167.6 °C, moving closer to the T_m of EMB. This shift indicated that EMB was tightly encapsulated in the PLA matrix, with molecular-level affinity and interaction between PLA and EMB, leading to the formation of a more homogeneous phase structure rather than a simple physical mixture or surface adsorption.[40,52] Moreover, Wu et al. confirmed that PLA and EMB exhibit a certain degree of compatibility, further supporting these findings.[9]

The crystallinity of PLA slightly increased from 32.72% to 34.69% upon EMB encapsulation. This slight increase can be explained by the fact that EMB may act as a heterogeneous nucleating agent, thereby promoting PLA recrystallization from the molten state.[9] A higher crystalline fraction of PLA makes it more difficult for EMB to disperse and penetrate the polymer matrix, thus lowering the drug loading and encapsulation efficiency.[8,9,40] In addition, PLA crystallinity not only influences encapsulation efficiency but also governs the release behavior of EMB. Specifically, EMB can diffuse more easily through the amorphous domains of PLA, whereas higher crystallinity hinders this diffusion, leading to a slower release rate. Furthermore, the degradation of PLA preferentially occurs in the amorphous regions.[54,55] In this study, PLA retained its semi-

Table 6 DSC characteristics of EMB and PLA microparticles with and without loading EMB

DSC results samples	EMB	PLA	EMB loaded PLA (PLA–EMB)
T_g, °C	—	69.5	69.2
C_{Pg}, J (g^{-1} K^{-1})	—	0.03543	0.6805
T_c, °C	—	103.8	103.9
C_{Pg}, J (g^{-1} K^{-1})	—	0.222	0.5193
ΔH_c, J g^{-1}	—	−6.942	−9.854
T_m, °C	150.3	168.4	167.6
C_{Pm}, J (g^{-1} K^{-1})	1.015	0.8001	1.509
ΔH_m J g^{-1}	—	37.4	42.15
χ_C (%)	—	32.72	34.69

crystalline nature with only a negligible change in crystallinity; therefore, the release profile of EMB was not significantly affected.

Fig. 6 presents the TG and DTG curves of EMB and PLA microparticles with and without EMB loading. EMB exhibited a slight weight loss (<1 wt.%) between 60 and 130 °C due to adsorbed moisture. Its major decomposition process started at 202.3 °C and extended over a broad temperature range (202–510 °C). The DTG profile revealed three T_{max} peaks at 216.3 °C, 272.9 °C, and 406.1 °C, corresponding to successive decomposition steps.[50,56] In contrast, neat PLA microparticles showed a sharp, single-step weight loss between 276.8 °C and 380 °C, with one T_{max} at 362.8 °C, indicating a rapid and concentrated decomposition process. For PLA microparticles encapsulating EMB, the TG curve became more gradual, while the DTG curve showed one T_{max} at a lower temperature (290 °C) with weaker intensity and a broader shoulder (251–460 °C). These observations indicate that the thermal stability of EMB was improved when encapsulated in PLA, as PLA acted as a thermally stable carrier that shielded EMB from direct degradation. However, at elevated temperatures, both PLA and EMB melted, and EMB leached out first, triggering the earlier decomposition of PLA. Taken together with the DSC results, these findings further confirm the strong interaction and mutual stabilization between PLA and EMB in the microparticles.

3.2.3. UV and thermal stabilities. The stability of EMB, either free or encapsulated in PLA microparticles, was evaluated through UV irradiation tests and accelerated storage at elevated temperature (54 °C). As shown in Fig. 7, both free and encapsulated EMB degraded progressively upon UV exposure. However, the degradation rate of free EMB was much faster and almost linear over time. After 7 days, the amount of free EMB decreased by approximately 86%, whereas encapsulated EMB only lost 24% under the same conditions. This clearly demonstrates the shielding effect of PLA, which prevents direct UV penetration and delays the photodegradation of EMB. A similar protective trend was observed during thermal storage stability (Fig. 7). After 14 days at 54 °C, free EMB showed a reduction of 38%, while the encapsulated form decreased by only 19%. The slower decomposition of encapsulated EMB can be attributed to the thermal barrier function of PLA, as confirmed by TG/DTG

analysis (Fig. 6), where PLA hindered heat transfer and retarded EMB volatilization and degradation.

Interestingly, in both UV and thermal stability tests, the initial degradation of encapsulated EMB occurred more rapidly during the first 4 days, as indicated by the steeper slope of the degradation curves (Fig. 7). This phenomenon was likely caused by the fraction of EMB adsorbed on the microparticle surface or located close to the outer layer of PLA, which was more vulnerable to external stress (UV photons or thermal energy). After this initial stage, the degradation slowed down significantly, suggesting that the majority of EMB entrapped within the PLA matrix was well protected against environmental factors.

For the majority of EMB entrapped deeper inside the microparticles, the PLA matrix provided an effective shielding effect, making them less susceptible to degradation. Consequently, the degradation of encapsulated EMB proceeded at a slower and more stable rate during the later stages of the test. This finding further confirms the protective role of PLA, where encapsulation significantly retarded the decomposition of EMB by reducing direct exposure to external thermal stress. When comparing the two stress conditions, UV irradiation exerted a much stronger effect on EMB degradation than elevated temperature, as reflected by the steeper slope of the degradation curves (Fig. 7). This highlights that photodegradation was the dominant pathway of EMB instability, while thermal degradation was relatively less severe within the investigated storage period.

3.3. *In vitro* release performances of the microparticles

Fig. 8 shows the cumulative release (Q) profiles of free EMB and EMB encapsulated in PLA microparticles in 50° alcohol (E50) and absolute alcohol (E100) solutions. The release of free (unencapsulated) EMB occurred very rapidly in both media. Within only 18 hours, free EMB was almost completely released, reaching Q values of 92.3% in E50 and 98.5% in E100, respectively. In contrast, the release of encapsulated EMB was markedly prolonged. To reach a similar release level, the required time was approximately 288 hours (12 days) in E50 and 264 hours (11 days) in E100, corresponding to 16-fold and 14.7-fold longer durations compared to free EMB in the respective media.
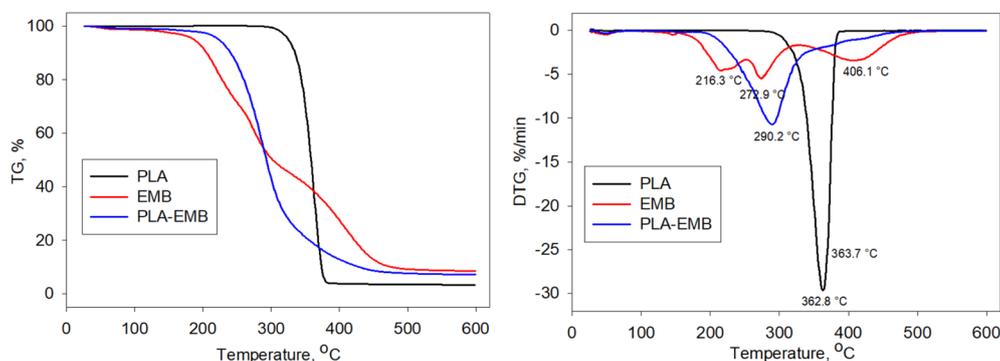

Fig. 6 TG and DTG diagrams of EMB and PLA microparticles with and without loading EMB.
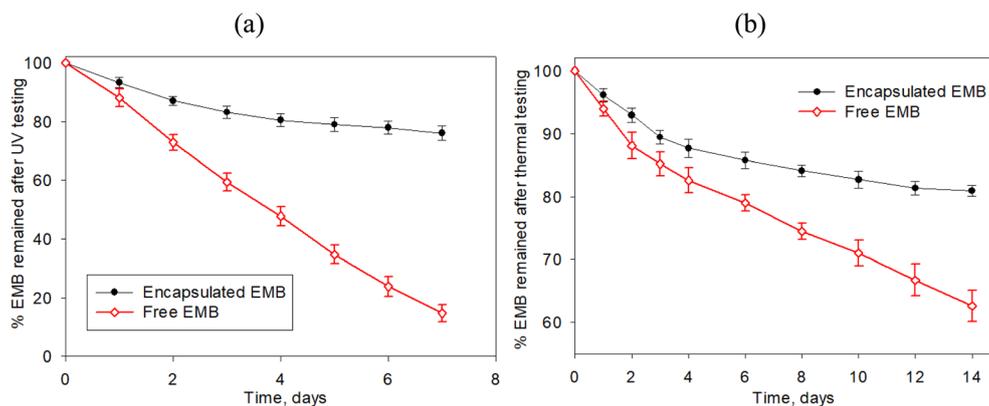
Fig. 7 Percent remaining weight of encapsulated and unencapsulated EMB after (a) 7 days of UV irradiation exposure and (b) 14 days of storage at 54 °C.
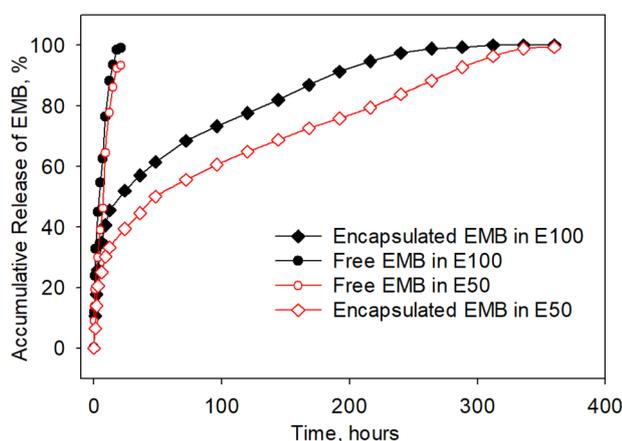

Fig. 8 The cumulative release of EMB from free form and PLA-encapsulated microparticles *versus* immersion time in 50° alcohol (E50) and absolute alcohol (E100).

These findings clearly demonstrate the significant sustained-release effect imparted by PLA encapsulation. Moreover, both free and encapsulated EMB exhibited faster release rates in absolute alcohol (E100) compared with 50° alcohol (E50), indicating that the release process was influenced by the polarity and solvation capacity of the medium.

At the early stage, the release of EMB from microparticles occurred rapidly, resembling a burst-release behavior. After 9 hours, the cumulative release (Q) reached 30.26% and 40.55% in E50 and E100, respectively. To achieve 50% release, the microparticles required approximately 48 hours in E50 and 24 hours in E100, almost coinciding with the burst-release phase. Although EMB exhibits low toxicity to humans and shows limited dispersion in soil and aquatic environments due to poor water solubility, it is highly toxic to aquatic organisms such as fish, crustaceans, and other invertebrates. Therefore, in field applications, the required dosage should be carefully calculated for this initial stage to maximize insecticidal efficiency while minimizing ecological residues. Because EMB can be easily decomposed by UV irradiation, sunlight, or environmental pH

changes, its long-term ecological impact is reduced, but so is its insecticidal efficacy.

In the later stage, the release rate slowed down gradually. As a result, the total time for complete release of encapsulated EMB extended 15–16 times longer than that of free EMB. This provides a strong basis for determining appropriate microparticle dosages to ensure effective pest control while reducing ecological impacts. According to Abdu Allah and Zhu, EMB has a half-life of about 6.2 days on leaves, corresponding to activity lasting around 7 days after spraying.[57,58] With a release duration 15–16 times longer than free EMB, PLA-encapsulated EMB is estimated to remain active for approximately three months. However, both the activity and persistence of EMB, whether free or encapsulated, are strongly dependent on environmental conditions. Thus, further laboratory toxicity tests, *in vivo* evaluations, and field trials are required to confirm the prolonged activity and ecological impact of EMB-loaded microparticles.

Yin *et al.*[8] reported that EMB release follows a first-order kinetic model of the form: $Q = a(1 - e^{-bt})$.

Applying this model to the present study yielded the following equations:

• Free EMB: $Q = 93.98(1 - e^{-0.01212t})$ with coefficient of determination $R^2 = 0.979$ for both in the alcohol 50° solution and absolute alcohol;

• Encapsulated EMB in E50: $Q = 87.48(1 - e^{-0.01686t})$ with $R^2 = 0.886$ in the alcohol 50° solution; and in the absolute alcohol.

• Encapsulated EMB in E100: $Q = 89.68(1 - e^{-0.03816t})$ with $R^2 = 0.885$.

The relatively high determination coefficients ($R^2 > 0.88$), especially for free EMB ($R^2 = 0.988$), confirm that both free and encapsulated EMB release processes fit the first-order model well. Among the parameters, coefficient a had a stronger influence on Q than coefficient b. The values of a decreased in the order: free EMB > encapsulated EMB in E100 > encapsulated EMB in E50, clearly demonstrating that encapsulation slowed the release compared with free EMB, and that release occurred faster in absolute alcohol than in 50° alcohol.

Since the release followed a first-order model, the process is governed primarily by the concentration of EMB remaining

inside the PLA microparticles. Hence, diffusion is the dominant release mechanism. EMB dissolves readily in ethanol and diffuses outward through the PLA matrix. This explains the burst release observed initially, where EMB molecules loosely adsorbed on or near the microparticle surface diffused rapidly into the solvent. The faster release in E100 than in E50 also results from the higher solubility of EMB in absolute ethanol.

At later stages, EMB molecules located deeper inside the PLA matrix required ethanol penetration into the microparticles before dissolution, making diffusion more difficult and slower. Although PLA swelling could potentially enhance diffusion, the industrial-grade, high-molecular-weight PLA used in this work is highly resistant to swelling in ethanol under room or elevated temperatures. Degradation of PLA through hydrolysis could also accelerate release, but PLA degradation typically requires more than six months (sometimes up to two years), far exceeding the release duration of EMB.[54,55,59,60] In alkaline conditions (pH > 9), PLA hydrolyzes faster, which could promote EMB release; however, such conditions may simultaneously accelerate EMB degradation, reducing pesticidal efficiency. Importantly, the biodegradability of PLA ensures no long-term environmental residues once EMB is fully released. Moreover, particle size also significantly influenced EMB release. The small average diameter (3.24 μm) increased the surface-to-volume ratio, enhancing solvent contact and reducing diffusion distance, thereby facilitating EMB release. Thus, PLA encapsulation slowed EMB release mainly by hindering ethanol penetration and diffusion, providing a controlled release system that prolongs insecticidal activity while mitigating ecological risks.

4. Conclusion

The findings of this work is the investigation of the optimized the preparation conditions of EMB-loaded PLA microspheres, with the best results obtained at a PLA solution concentration of 6%, an EMB/PLA weight ratio of 50/100, and a gelatin-polyvinyl alcohol mixture as surfactant. The resulting microspheres exhibited an average particle size of 3.24 μm, an EMB loading content of 28.74%, and an encapsulation efficiency of 86.23%. Encapsulation significantly enhanced the UV and thermal stabilities of EMB, while *in vitro* release experiments demonstrated a much slower and controllable release profile compared to free EMB. This sustained release prolonged the activity and extended the effective lifetime of EMB. Overall, these formulations show great promise as a smart pesticide system that improves EMB utilization efficiency and contributes to sustainable agricultural practices. Further studies on toxicity and *in vivo* performance will be conducted to fully assess their potential applications.

Conflicts of interest

There are no conflicts to declare.

Data availability

The authors confirm that the data supporting the findings of this study are available within the article.

Supplementary information: providing details on materials, determination of emamectin benzoate (EMB) loading content (LC) and encapsulation efficiency (EE) by UV-Vis spectroscopy, as well as *in vitro* release testing. Additional results, including digital microscopic images, UV-Vis absorption spectra, DLS diagrams, and FTIR spectra, are also presented. See DOI: **https://doi.org/10.1039/d5ra03833b**.

References

1 J. R. Lamichhane, *Crop Prot.*, 2017, **97**, 1–6.
2 M. Tudi, H. Daniel Ruan, L. Wang, J. Lyu, R. Sadler, D. Connell, C. Chu and D. T. Phung, *Int. J. Environ. Res. Public. Health.*, 2021, **18**(3), 1112.
3 V. De Luca, L. Mandrich and G. Manco, *Life*, 2023, **13**, 490.
4 X. Ding, F. Gao, L. Chen, Z. Zeng, X. Zhao, Y. Wang, H. Cui and Bo Cui, *ACS Appl. Mater. Interfaces*, 2024, **16**(17), 22558–22570.
5 S. Song, Y. Wang, J. Xie, B. Sun, N. Zhou, H. Shen and J. Shen, *ACS Appl. Mater. Interfaces*, 2019, **11**(37), 34258–34267.
6 D. Yang, B. Cui, C. Wang, X. Zhao, Z. Zeng, Y. Wang and H. Cui, *J. Nanomater.*, 2017, 1–9.
7 F. Gao, B. Cui, C. Wang, X. Li, B. Li, S. Zhan, Y. Shen, X. Zhao, C. Sun, C. Wang, Y. Wang, Z. Zeng and H. Cui, *Pest. Manag. Sci.*, 2022, **78**(8), 3717–3724.
8 M. Yin, X. Zhu and F. Chen, *J. Integr. Agric.*, 2018, **17**(3), 640–647.
9 S. Xu, Y. Liu, Y. Chen and G. Wu, *Molecules*, 2024, **29**, 6008.
10 R. Tao, C. You, Q. Qu, X. Zhang, Y. Deng, W. Ma and C. Huang, *Environ. Sci.: Nano*, 2023, **10**, 351–371.
11 A. Bratovcic, W. M. Hikal, H. A. H. Said-Al Ahl, K. G. Tkachenko, R. S. Baeshen, A. S. Sabra and H. Sany, *Open J. Ecol.*, 2021, **11**, 301–316.
12 S. Rajna, A. U. Paschapur and K. V. Raghavendra, *Indian Farmer*, 2019, **6**(1), 17–21.
13 L. Feng, B. Cui, D. Yang, C. Wang, Z. Zeng, Y. Wang, C. Sun, X. Zhao and H. Cui, *J. Nanomater.*, 2016, **3**, 1–7.
14 C. H. Zheng, *Anhui Chem. Ind.*, 2012, **38**(3), 49–51.
15 M. Guo, W. Zhang, G. Ding, D. Guo, J. Zhu, B. Wang, D. Punyapitak and Y. Cao, *RSC Adv.*, 2015, **5**, 93170–93179.
16 Q. Shang, Y. L. Shi, Y. H. Zhang, T. Zheng and H. Y. Shi, *Polym. Adv. Technol.*, 2013, **24**, 137–143.
17 X. Cheng, X. Liu, H. Wang, X. Ji, K. Wang, M. Wei and K. Qiao, *PLoS One*, 2015, **10**(10), e0141235.
18 C. Dowler, O. Dailey and B. Mullinix, *J. Agric. Food Chem.*, 1999, **47**, 2908–2913.
19 A. Elabasy, A. Shoai, M. Waqas, M. Jiang and Z. Shi, *Molecules*, 2019, **24**, 2801.

20 K. Shiomori, J. Taniguchi, S. Kiyoyama, Y. Kawano and H. Hatate, *J. Chem. Eng. Jpn.*, 2004, **37**(2), 357–364.

21 F. Sopea, C. Maqueda and E. Morillo, *Cien. Inv. Agr.*, 2009, **35**(1), 27–42.

22 R. Meng, S. Liu, R. Zhu, X. Zhou, L. Bai and X. Li, *Chin. J. Pesticide Sci.*, 2012, **14**(5), 565–573.

23 D. Liu, S. Zhang, C. Zhang, S. Yang, B. Huang and G. Wu, *Agrochem*, 2013, **52**(1), 19–23.

24 D. Li, B. Liu, F. Yang, X. Wang, H. Shen and D. Wu, *Carbohydr. Polym.*, 2016, **136**(20), 341–349.

25 B. Liu, Y. Wang, F. Yang, H. Cui and D. Wu, *J. Agric. Food Chem.*, 2018, **66**(26), 6561–6568.

26 J. Suave, E. C. Dall'Agnol, A. P. T. Pezzin, M. M. Meier and D. A. K. Silva, *J. Appl. Polym. Sci.*, 2010, **117**(6), 3419–3427.

27 C. Lin, L. Liu, Y. Liu and J. Leng, *Compos. Struct.*, 2022, **279**, 114729.

28 B. Liu, Y. Wang, F. Yang, g X. Wan, H. Shen, H. Cui and D. Wu, *Colloids Surf., B*, 2016, **144**, 38–45.

29 R. Guo, B. Huang, X. Yang, Z. Wu and G. Wu, *Chin. J. Pesticide Sci.*, 2011, **13**(4), 409–414.

30 Y. Li, J. Dai, D. Cao, Y. Ma, L. Zhen and F. Chang, *IOP Conf. Ser.: Mater. Sci. Eng.*, 2020, **711**, 012026.

31 F. Barrera-Méndez, D. Miranda-Sánchez, D. Sánchez-Rangel, I. Bonilla-Landa, B. Rodríguez-Haas, J. L. Monribot-Villanueva and J. L. Olivares-Romero, *J. Mex. Chem. Soc.*, 2019, **63**(1), 50–60.

32 J. Yang, J. Feng, C. Sun, W. Chen, Y. Ma, Z. Chen, S. Dong and W. Deng, *J. Polym. Environ.*, 2021, **29**, 3145–3153.

33 S. Sun, X. Yang, L. Xu, J. Zhang, Y. Wang and Z. Zhou, *Sci. Total Environ.*, 2023, **862**, 160904.

34 Y. Li, D. Cao, F. Jia, F. Chang, R. Lv and J. Dai, *Mater. Lett.*, 2020, **264**, 127345.

35 C. Wang, K. Qiao, Y. Ding, Y. Liu, J. Niu and H. Cao, *Int. J. Biol. Macromol.*, 2023, **253**(Pt. 1), 126425.

36 G. Antonioli, G. Fontanella, S. Echeverrigaray, A. P. Longaray Delamare, G. Fernandes Pauletti and T. Barcellos, *Food Chem.*, 2020, **326**, 126997.

37 S. Freitas, H. P. Merkle and B. Gander, *J. Control. Release*, 2005, **102**(2), 313–332.

38 H. Zheng, D. Liu, H. Mou, S. Yang, C. Zhang, B. Huang and G. Wu, *Chin. J. Pesticide Sci.*, 2012, **14**(5), 557–564.

39 Y. Wang, A. Wang, C. Wang, B. Cui, C. Sun, X. Zhao, Z. Zeng, Y. Shen, F. Gao, G. Liu and H. Cui, *Sci. Rep.*, 2017, **7**(1), 12761.

40 S. F. Zhang, P. H. Chen, F. Zhang, Y. F. Yang, D. K. Liu and G. Wu, *J. Agric. Food Chem.*, 2013, **61**(50), 12219–12225.

41 Y. Yang, Y. Ning, C. Wang and Z. Tong, *Polym. Chem.*, 2013, **4**, 5407–5415.

42 A. Wang, Y. Wang, C. Sun, C. Wang, B. Cui, X. Zhao, et al., *Nanoscale Res. Lett.*, 2018, **13**(1), 2.

43 S. Morsy, *Int. J. Curr. Microbiol. App. Sci.*, 2014, **3**(5), 237–260.

44 S. İmamoğlu, B. D. Gökberk, M. Eryılmaz and A. Bozkır, *J. Res. Pharm.*, 2022, **26**(5), 1156–1176.

45 S. A. Guhagarkar, V. C. Malshe and P. V. Devarajan, *AAPS. Pharm. Sci. Tech.*, 2009, **10**(3), 935–942.

46 P. E. Kamdem, I. Sandrine, N. Bouelet and S. Isabelle, *Int. J. Sci. Basic Appl. Res.*, 2014, **17**(1), 74–94.

47 H. Y. Chi, N. Y. Chang, C. Li, V. Chan, J. H. Hsieh, Y. H. Tsai and T. Lin, *Polymers*, 2022, **14**(13), 2610.

48 A. Mushtaq, S. Mohd Wani, A. R. Malik, A. Gull, S. Ramniwas, G. Ahmad Nayik, S. Ercisli, R. Alina Marc, R. Ullah and A. Bari, *Food Chem. X.*, 2023, **18**, 100684.

49 N. F. Ibadat, C. M. Ongkudon, S. Saallah and M. Misson, *Polymers*, 2021, **13**, 3639.

50 A. Elabasy, A. Shoaib, M. Waqas, M. Jiang and Z. Shi, *Molecules*, 2019, **24**(15), 2801.

51 J. Panyam, D. Williams, A. Dash, D. Leslie-Pelecky and V. Labhasetwar, *J. Pharm. Sci.*, 2004, **93**(7), 1804–1814.

52 J. D. Badia, L. Santonja-Blasco, A. Martínez-Felipe and A. Ribes-Greus, *Polym. Degrad. Stab.*, 2012, **97**, 1881–1890.

53 F. R. Beltrán, M. U. de la Orden, V. Lorenzo, E. Pérez, M. L. Cerrada and J. Martínez-Urreaga, *Polymer*, 2016, **107**, 211–222.

54 V. Skorokhoda, I. Semeniuk, T. Peretyatko, V. Kochubei, O. Ivanukh, Y. Melnyk and Y. Stetsyshyn, *Polymers*, 2025, **17**, 675.

55 D. V. Cong, T. Hoang, N. V. Giang, N. T. Ha, T. D. Lam and M. Sumita, *Mater. Sci. Eng. C*, 2012, **32**, 558–563.

56 B. B. Huang, D. X. Liu, D. K. Liu and G. Wu, *Molecules*, 2019, **24**, 4315.

57 G. Abdu-Allah, *Afr. Entomol.*, 2011, **19**(3), 733–737.

58 M. Li, W. Chen, M. Li and L. Han, *Bull. Environ. Contam. Toxicol.*, 2011, **87**(6), 699–702.

59 B. B. Huang, S. F. Zhang, P. H. Chen and G. Wu, *Sci. Rep.*, 2017, **7**(1), 10864.

60 R. B. Rajesh, R. Saraswathy, S. Avunje, R. A. Raja, P. Kumararaja, P. K. Patil and J. Asian, *Environ. Ecol.*, 2024, **23**(10), 38–48.